International Journal of Microwave and Wireless Technologies

cambridge.org/mrf

A compact and economical AMC backed antenna solution for wearable biomedical applications

Mohit Yadav[1], Muquaddar Ali[2] and R. P. Yadav[1]

[1]Department of Electronics and Communication Engineering, Malaviya National Institute of Technology, Jaipur, India and [2]JECRC University, Jaipur, India

Research Paper

Cite this article: Yadav M, Ali M, Yadav RP (2023). A compact and economical AMC backed antenna solution for wearable biomedical applications. *International Journal of Microwave and Wireless Technologies* **15**, 1514–1523. https://doi.org/10.1017/S1759078723000211

Received: 12 September 2022
Revised: 1 March 2023
Accepted: 8 March 2023

Keywords:
AMC Reflector; Biomedical applications; High Gain; ISM Band; Monopole; SAR; Wearable antenna system

Corresponding author:
Mohit Yadav,
E-mail: 2018rec9041@mnit.ac.in

Abstract

A rectangular monopole antenna with an extended ground, excited by Coplanar Waveguide (CPW) and backed by a 6×6 array of fractal artificial magnetic conductor (AMC) unit cells, resonating at 5.8 GHz in Industrial, Scientific, and Medical (ISM) band, is presented in this manuscript. To attain the objective of proposing a compact and economical antenna solution for employment in wearable biomedical domain, a novel approach of utilizing both surfaces of the same dielectric for engraving antenna element as well as AMC array is adopted. It results in the elimination of layers of expensive substrate (RO3003) and of thick separator (foam) between antenna and AMC array. During measurement in open space, the proposed antenna system exhibited an impedance bandwidth of 570 MHz with a gain of 7.9 dBi. While a total realized gain of 7.5 dBi, amounting to a gain enhancement of about 3 dB as compared to that of monopole alone, is observed when the integrated antenna system is placed just over a three-layer rectangular human body equivalent model. Specific absorption rate values, as calculated at 5.8 GHz and averaged over 1 and 10 g of human tissue, are 0.0117 and 0.00244 W/kg, respectively. Obtained results strongly advocate the use of the proposed antenna system in smart wearable healthcare devices.

Introduction

Communication, i.e. exchange of information, has been the very foundation of the development of human civilization. The ever-growing communication technology starting from the use of sign languages like smoke signals, cave paintings, etc., as initial modes of communication, has reached another level by making it possible the transmission of real-time physiological data of human beings, enabling them to take crucial decisions concerning their well-being. The real-time monitoring and transmission of these data are facilitated by the use of a Wireless Body Area Network (WBAN), a network of wireless communicating devices which are either implanted into (invasive) or worn over the human body (non-invasive) [1]. A wide range of applications adding comforts to the lives of living beings, including smart healthcare monitoring, infotainment, smart rescue systems, GPS-enabled smart shoes, etc., are being offered by WBANs [2–4], making it a topic of interest among researchers. Researchers are working tirelessly to provide novel solutions for sensors, power requirements, and antenna systems to be employed in these smart wearable electronic devices.

The operating environment of wearable antennas makes the task of designing these antennas quite challenging. Due to the dielectric nature of human tissues, the performance of on-body antennas is likely to be affected very badly. Another important task is to minimize the electromagnetic absorption by human tissues so as to comply with the safety standards of specific absorption rate (SAR). Moreover, the antenna system needs to be conformal, flexible, and compact enough to fit into a small space over the human body surface.

A variety of flexible substrates like textiles, polyester films, polymer composites like Polydimethylsiloxane (PDMS) -coated silica nanoparticles [5], and polymer yarns [6] have been utilized to design planar monopole antenna, planar inverted-F antenna, microstrip patch antenna [7–10], etc., for employment in WBANs. But, due to a lack of proper isolation from the human body, these antennas suffer from some serious drawbacks such as impedance mismatching, frequency detuning, efficiency degradation, and distorted radiation patterns.

To overcome these drawbacks, meta-surfaces like arrays of artificial magnetic conductor (AMC)/ High Impedance Surface (HIS) unit cells are being utilized by researchers as antenna reflectors [11–17]. An increase in the array size up to a certain limit results in improved radiation performance of the structure [18, 19]. So one of the many challenges before researchers is also to realize novel compact AMC structures to be used as reflectors.

A CPW-fed reconfigurable folded slot antenna with a 3×3 AMC array as reflector [20] demonstrated gains of 6.4 dBi at 2.45 GHz and 3 dBi at 3.3 GHz. Each of the substrates

used for the antenna and AMC is 1.52 mm in thickness, while the antenna and AMC are separated by a considerable gap of 6.25 mm. Thus, making the overall structure quite thick (>9 mm), which is obviously undesirable in the wearable domain. At 5.8 GHz, a sufficiently large gain of 7.47 dBi is reported in [21] when the antenna backed by AMC surface is placed at a distance of 3 mm from the body equivalent. AMC-backed dual-band monopole [22] provided the gain of 5.2 and 7.7 dBi at 2.45 and 5.8 GHz, respectively. Relatively larger gains of 9.4 and 6.6 dBi at 3.5 and 5.8 GHz, respectively, are demonstrated by a dual-band (3.5 and 5.8 GHz) monopole backed by a 4×4 AMC [19]. A monopole antenna with 1×2 textile-based AMC backing provided a gain of 4 dBi at 2.4 GHz [23]. A multi-band antenna integrated with 5×5 AMC [24] provided gain enhancements of 4.93, 5.92, 5.54, and 4.95 dB at 2.45, 3.5, 4.6, and 5.8 GHz, respectively. But, a 23 mm gap between the antenna and AMC outsizes the overall structure. At 2.45 GHz, a gain of 6.6 dBi is obtained from a monopole antenna utilizing a 3×3 array of textile electromagnetic band gap material as a reflector [25]. Sufficiently high gains of 6.71 and 7.82 dBi at 3.5 and 5.8 GHz, respectively, are obtained from a fully textile triangular monopole antenna backed by a 2×2 textile AMC array [26]. [27] Proposes a patch antenna backed by a 3×3 AMC array, demonstrating gains of 4.88 and 4.73 dBi at 2.45 and 5.8 GHz, respectively. Gains of 5.9 and 6 dBi are obtained at 3.5 and 5.8 GHz, respectively, from a 3×3 polarization rotation AMC backed dual band monopole [28].

A comprehensive study of the research works discussed above suggests improvements in the design of wearable antennas so as to bring compactness to the final integrated structure. This study, therefore, also acts as a guiding light for the research work presented in this manuscript. In fact, the novelty of the presented work originates from the very objective of proposing a compact and economical antenna solution for wearable applications. In order to achieve this objective, it was thought to utilize the same substrate for both antenna and AMC array. This thought has been materialized by having a monopole antenna on one surface of the substrate while an array of fractal AMC unit cells on the other surface of the same substrate, thereby eliminating two layers, one of the expensive substrate (RO3003), while another one is of thick separator (usually foam) between AMC array and antenna. The implementation of this novel approach results in an economical and compact, low profile solution for integrated antenna systems to be utilized in the wearable domain.

Rest of the paper is organized as follows: section "Design of wearable antenna system" presents the geometry of the proposed antenna, AMC unit cell, and the integrated antenna structure. Fabricated prototype and a comparison between measured and simulated results in both flat as well as bending scenarios are presented in section "Fabrication and measurement". Section "On body performance and comparison with recent works" discusses the performance of the integrated antenna in an equivalent human body environment and its comparison with some of the recent research works is also presented here. Finally, a conclusive summary of the research work with some of its future prospects is provided in section "Conclusion and future scope".

Design of wearable antenna system

Designs of all the constituents of the proposed antenna system, namely the monopole, the AMC unit cell, and the final integrated structure itself, are discussed in this section. Corresponding simulated results of scattering parameter (S_{11}), radiation pattern, reflection phase diagram for the AMC unit cell along with conformability tests on the integrated antenna, and an analytical study to understand the effects of AMC array size and spacing between AMC unit cells in the array, on different performance parameters of the proposed antenna, are also included in this section. A flow chart depicting the design flow of the proposed wearable antenna system is presented in Fig. 1.

Design of monopole with extended ground

Inspired by [25], a CPW-fed rectangular monopole antenna with an extended ground plane is designed to have resonance in the ISM band at 5.8 GHz in order to serve for wearable biomedical applications. The layout of the proposed antenna is displayed in Fig. 2(a). The Ansys HFSS software is used to design the antenna over a substrate of RO 3003. The substrate thickness is taken to be 0.787 mm, while its relative permittivity is 3. It consists of a square patch with W_{patch} as the length of its side; two slots of width W_{cut} and length L_{cut} are cut from the patch in order to facilitate inset feeding at a distance of L_{cut} from the feed line. The ground layer of CPW is extended in such a way that the patch and ground are separated by g_1, while g_{feed} is the separation between the ground and CPW feed line of width W_{feed}. A gap of gg is maintained between the interface of the SMA connector and the feed line so that only the CPW ground plane touches the outer part of the SMA connector. The parameters used in the proposed design, along with their optimized values are tabulated in Table 1.

It can be observed from the reflection profile of the proposed monopole (Fig. 2(b)) that the antenna resonates at 5.93 GHz with a bandwidth of 330 MHz, extending from 5.76 to 6.09 GHz. Figure 2(c) reveals that the antenna has a bidirectional radiation pattern with peak gain of 4.6 dBi, but a very low front-to-back ratio (FBR) of 1.6 dB.

Parametric study

Some of the key parameters affecting the resonance frequency of the antenna are W_{patch}, g_1, and L_{cut}. Parametric studies are performed to get the optimum values of these parameters. In order to provide an insight of the antenna design and to convey a better understanding about the effect of parameters on the resonance frequency of the antenna, readers are provided with Figs 3(a)–3(c), displaying the reflection profile of the antenna for different

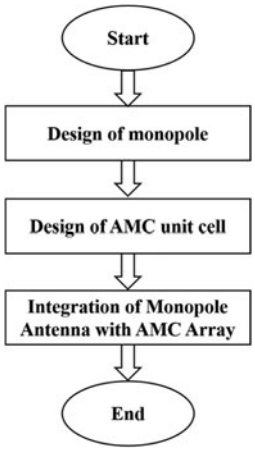

Figure 1. Design flow of wearable antenna system.

https://doi.org/10.1017/S1759078723000211 Published online by Cambridge University Press

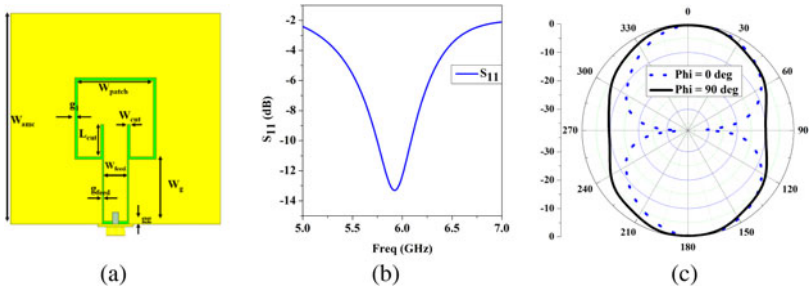

Figure 2. (a) Monopole antenna with extended ground, (b) reflection coefficient, and (c) radiation pattern.

Table 1. Design dimensions of monopole with extended ground

Variable name	Value (mm)	Variable name	Value (mm)
g_1	0.75	W_{amc}	36
g_{feed}	0.3	W_{cut}	0.5
gg	0.5	W_{feed}	4
h	0.787	W_g	10.75
L_{cut}	5	W_{patch}	13.5

parametric variations. As depicted in Fig. 3(a), the resonant frequency of the antenna is inversely proportional to the width of the patch W_{patch}. The gap g_1 between the extended ground and the patch affects the impedance matching to a large extent as illustrated in Fig. 3(b). Like in a normal microstrip patch antenna, the length of inset feed can be controlled for improving the impedance matching as shown in Fig. 3(c).

Antenna operated in equivalent human body environment

In order to test the designed monopole antenna for its employability in wearable biomedical devices, the antenna needs to be simulated in an equivalent human body environment. For this purpose, a three-layer rectangular human body equivalent model of size 90 mm × 90 mm × 33 mm [19] is designed in HFSS, as shown in Fig. 4(a). Different layers as seen from the top are skin with a thickness of 2 mm, 8 mm thick fat layer, and lastly the muscle layer with a thickness of 23 mm. Characteristics of all the three layers of human tissues at 5.8 GHz are provided in Table 2 [29–31].

The reflection profile of the antenna when placed at variable distances from the equivalent human body model is recorded in each case and is presented for comparison in Fig. 4(b). It can be seen that the antenna retained its resonance characteristics at a distance of 12 mm from the human body model, but it would outsize the antenna system to a large extent. For any antenna to be able to qualify for employment in human body environment, the reduction of this separation between human body and antenna system is also of utmost importance along with other specific requirements like increasing its gain, FBR or achieving unidirectional radiation pattern, and to obtain a low SAR value. To achieve these objectives, placement of some sort of reflecting surface of periodically arranged AMC unit cells as a backing element to the antenna is envisaged. The subsequent section contains the design and simulation of the AMC unit cell.

Design of AMC unit cell

AMC structure is designed using an iterative process, where scaled versions of the central square patch are connected at all its corners. Second-order fractal geometry with a scaling factor of 0.5 is used in the proposed design. Foam of height h_{amc1}, having a dielectric constant of 1.05, is used to separate the ground and AMC structure. A substrate area of size $6 \times 6\ \text{mm}^2$, encompassing the final geometrical structure of the unit cell, is depicted in Fig. 5(a).

Table 3 lists the optimized values of different design parameters. Simulation has been carried out in HFSS using a waveguide analytical model, wherein master–slave boundary conditions are applied on four walls of the waveguide, and a Floquet port is used on its top surface (Fig. 5(b)). Floquet port is de-embedded to the surface of the AMC unit cell in order to measure the reflection phase just above the AMC surface. It is to be noted here that the height of the waveguide must be at least a quarter of the wavelength of the AMC structure.

Reflection properties of the designed unit cell are exhibited in Fig. 6. Zero degree crossover frequency also referred to as the resonant frequency of AMC is 5.83 GHz with a wide bandwidth of

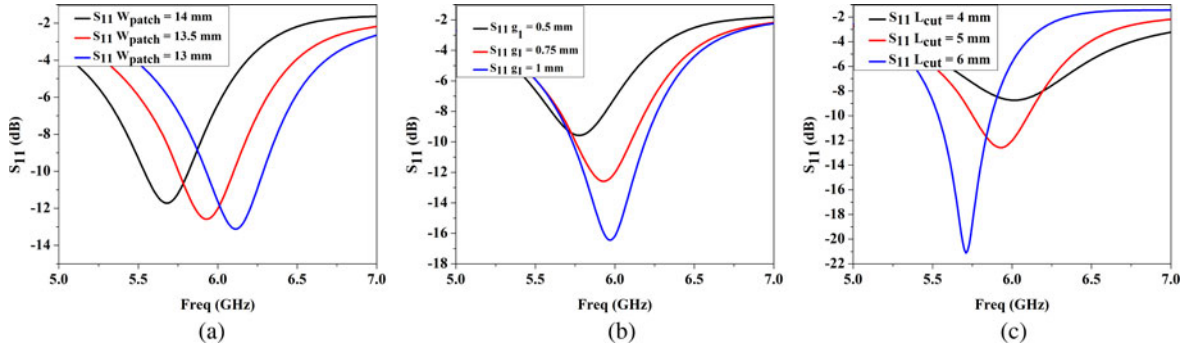

Figure 3. Reflection profile of the antenna with respect to parametric variations in (a) W_{patch}, (b) g_1, and (c) L_{cut}.

https://doi.org/10.1017/S1759078723000211 Published online by Cambridge University Press

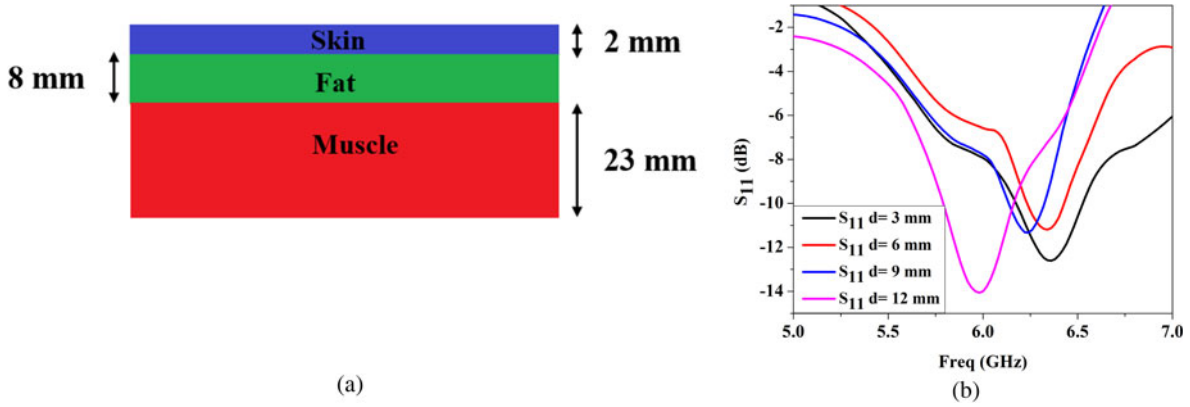

Figure 4. (a) Three-layer equivalent human body model, and (b) reflection profile of antenna in equivalent human body environment.

Table 2. Characteristics of human tissues at 5.8 GHz

Human tissue at 5.8 GHz	Dry skin	Fat	Muscle
Relative permittivity	35.114	4.9549	48.485
Conductivity (S/m)	3.717	0.29313	4.9615
Mass density (kg/m^3)	1090	930	1050

Table 3. Design parameters of AMC unit cell

Variable name	Value (mm)
h_{amc1}	3
W_{amc1}	6
W_{m0}	3
W_{m1}	1.5
W_{m2}	0.75

57% or 3.45 GHz (4.33–7.78 GHz). The increased height of the unit cell, i.e. the height of the foam, provides a large impedance (>65 KΩ) at zero crossover point, resulting in a broad bandwidth. Foam being inexpensive does not increase the overall cost.

Monopole integrated with reflector

An integrated antenna system, combining monopole with a reflective surface having a 6 × 6 array of AMC unit cells, is discussed here. As stated earlier, monopole and AMC array are engraved on both sides of the same substrate, having a thickness of 0.787 mm. The final integrated structure contains a rectangular layer of foam with a thickness of 3 mm, embedded between the AMC array and a very thin copper layer of 0.03 mm thickness, attached to the lower surface of the foam to serve the purpose of the ground. The total volume of the integrated antenna structure comes out to be $36 \times 36 \times 3.8$ mm^3. The final layout (Fig. 7) displays different layers of the integrated antenna structure. The first layer (cooper) is the ground layer, the second layer (foam) acts as a dielectric for the AMC array, the third layer (copper) is of AMC array, the fourth layer is of the antenna substrate RO 3003, and the fifth layer (copper) contains antenna geometry.

From parametric studies, the optimal reflector's size and optimal spacing between AMC unit cells in the array (*gap*) are found to be 6 × 6 and 0.7 mm, respectively. The remaining design parameters are tabulated in Table 4.

Effect of the size of AMC array/reflector

As gain and FBR are some of the vital parameters as far as the application domain of the designed antenna is considered. So, the effects of variations in the size of AMC array on these parameters at the operating frequency of the integrated antenna are studied and respective results are compiled in Table 5. Starting from a 2 × 2 AMC array, improvements in gain and FBR of the antenna are observed with an increase in the size of the reflector up to 6 × 6 array. Going beyond, 6 × 6 array size results in decreased gain and FBR. Therefore, the study provides reflector size of 6 × 6 array as the optimal one.

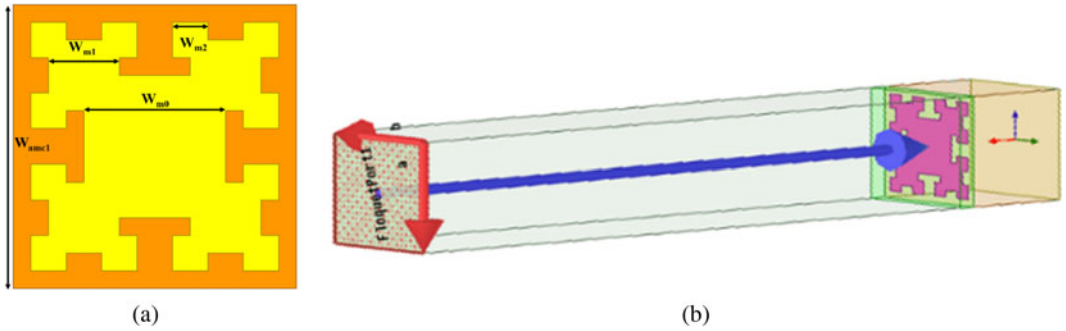

Figure 5. (a) Proposed AMC unit cell, and (b) simulation setup.

https://doi.org/10.1017/S1759078723000211 Published online by Cambridge University Press

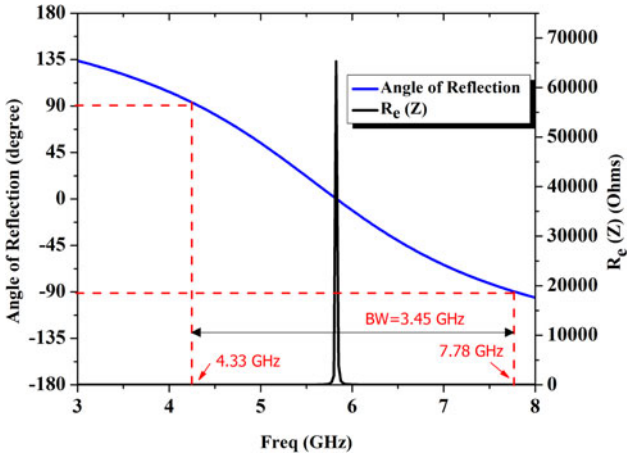

Figure 6. Angle of reflection and impedance of AMC unit cell.

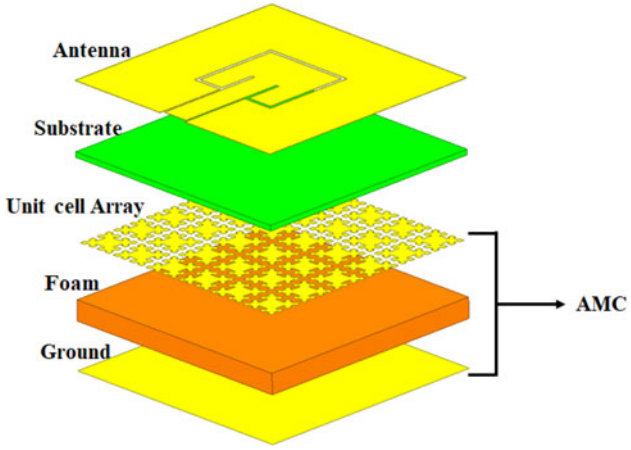

Figure 7. Multilayer view of integrated antenna.

Effect of the spacing between AMC unit cells

Once the size of AMC array is fixed, spacing between AMC unit cells is varied from 0.5 to 0.7 mm in steps of 0.1 mm each, and corresponding changes in the reflection profile of integrated antenna are observed as shown by the graph in Fig. 8. Slight variations in resonant frequency and impedance matching are seen. Proposed design uses a gap of 0.7 mm, as desired antenna performance is achieved quite well at this gap.

Test of conformability

Investigations regarding conformability of the designed antenna are performed by wrapping it over a PVC plastic cylinder (Fig. 9(a)). A study of the impacts of bending on the reflection coefficient of the antenna (Fig. 9(b)) shows little variations in impedance matching and resonant frequency, and therefore suggests that the proposed design has a quite stable reflection profile under different bending conditions.

Fabrication and measurement

Fabrication of the proposed antenna structure, along with its measured performance, is presented in this section. Rogers RO 3003, a semi-flexible substrate characterized by a dielectric constant of 3 and a loss tangent of 0.0013, having a thickness of 0.787 mm is utilized to engrave monopole on one of its surfaces while AMC array on the other surface, using general lithography.

Table 4. Design dimensions.

Variable name	Value (mm)	Variable name	Value (mm)
g_1	0.75	W_{cut}	0.5
g_{feed}	0.3	W_{feed}	4
gg	0.5	W_g	10.75
h	0.787	W_{m0}	3
h_{amc2}	3	W_{m1}	1.5
L_{cut}	5	W_{m2}	0.75
W_{amc}	36	W_{patch}	13.5
W_{amc1}	6	t_1	0.03

Table 5. Effect of the size of AMC array/reflector

Size of AMC array/ reflector	Frequency (GHz)	Gain (dBi)	FBR (dB)
2 × 2	5.78	6.8	7.2
3 × 3	5.76	7.1	7.5
4 × 4	5.81	7.2	8
5 × 5	5.9	7.3	10
6 × 6	5.81	7.9	14.8
7 × 7	5.7	5.1	11

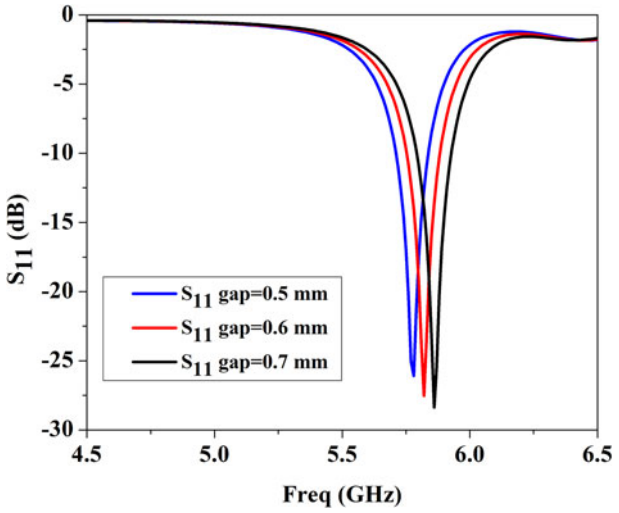

Figure 8. Effect of the spacing between AMC unit cells on reflection profile.

Measurement of S_{11} and gain in flat scenario

Fabricated layers of the integrated antenna are demonstrated in Fig. 10. Figure 10(a) represents the top layer of the laminate containing antenna geometry, while the AMC array printed on its bottom surface is shown in Fig. 10(b). The opposite surface of the copper foil shown in Fig. 10(c) is attached to the foam,

https://doi.org/10.1017/S1759078723000211 Published online by Cambridge University Press

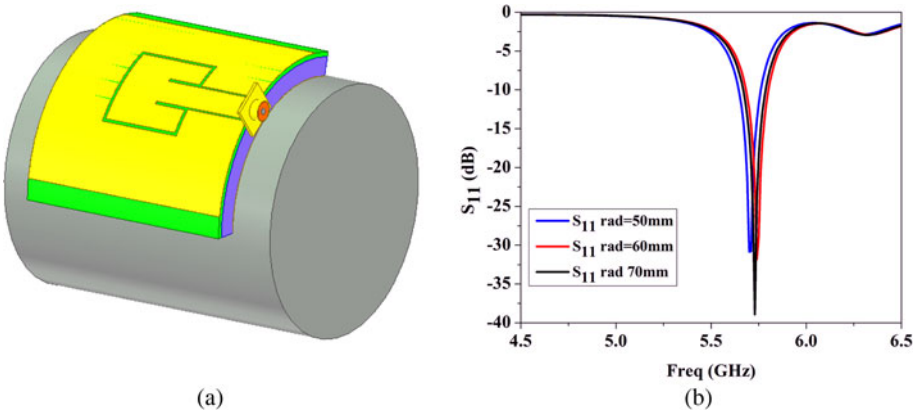

Figure 9. (a) Setup for conformability testing, and (b) effects of bending on reflection profile.

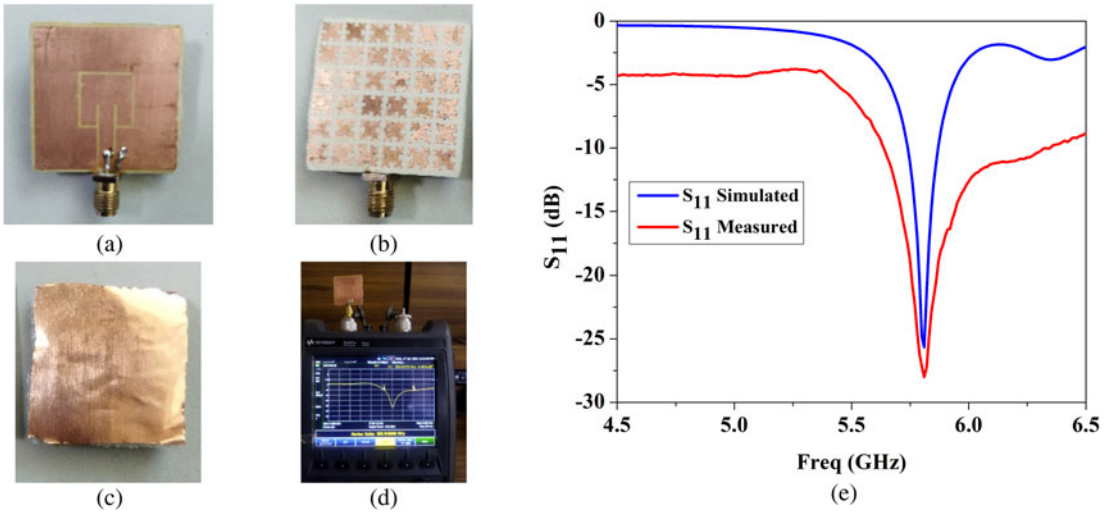

Figure 10. (a) Top monopole layer, (b) AMC reflector surface, (c) copper foil over foam, (d) antenna in the measurement environment, and (e) comparison between simulated and measured reflection coefficient.

embedded between the AMC array and copper foil in the integrated design.

Setup for the measurement of reflection coefficient using Keysights' handheld Vector Network Analyzer (VNA) N9914A is displayed in Fig. 10(d). Simulated and measured results of reflection coefficients exhibiting a high degree of coherence among them are represented in Fig. 10(e). Impedance bandwidth of the structure encompasses the desired ISM band very well, from 5.74 to 5.87 GHz with center frequency at 5.81 GHz.

Simulated and measured radiation patterns of the integrated antenna at resonant frequency 5.8 GHz in azimuth and elevation plane are displayed in Figs 11(a) and 11(b), respectively. Incorporation of AMC array as a reflector brings unidirectivity in the radiation pattern, thereby improving the peak gain to 7.9 dBi while FBR also improves to 14.8 dB.

Measurement of S_{11} and gain in bending scenario

Conformability tests performed through simulation are again verified by wrapping the fabricated antenna around a PVC plastic mug having a radius of 40 mm, as shown in Fig. 12(a). Corresponding simulated and measured results of reflection coefficient and radiation patterns are displayed in Figs 12(b)–12(d). Measured results are found to be in good agreement with simulated ones, suggesting that the proposed antenna design operates well under bending conditions without sacrificing its performance. As impedance matching deteriorates to some extent with bending, so in the bending scenario, the antenna gain reduces slightly by 0.5 dB in comparison to the gain measured in flat scenario. The measured and simulated results show that the FBR is 14.5 dB.

On body performance and comparison with recent works

In this section, the proposed antenna design is evaluated for its performance in an equivalent human body environment. Measurement of scattering parameter (S_{11}) performed on a human hand, SAR results, and a comparison of the proposed design with some of the recent state-of-the-art research works are also presented in this section. Simulations have been carried out after placing the integrated antenna just over the equivalent human tissue model of Fig. 4(a), and respective results are conveyed in the subsections to follow.

On body profile of reflection coefficient

The integrated antenna is evaluated for its performance over the human body by placing it over the human hand (Fig. 13(a)). Figure 13(b) presents the comparison of these measured results

https://doi.org/10.1017/S1759078723000211 Published online by Cambridge University Press

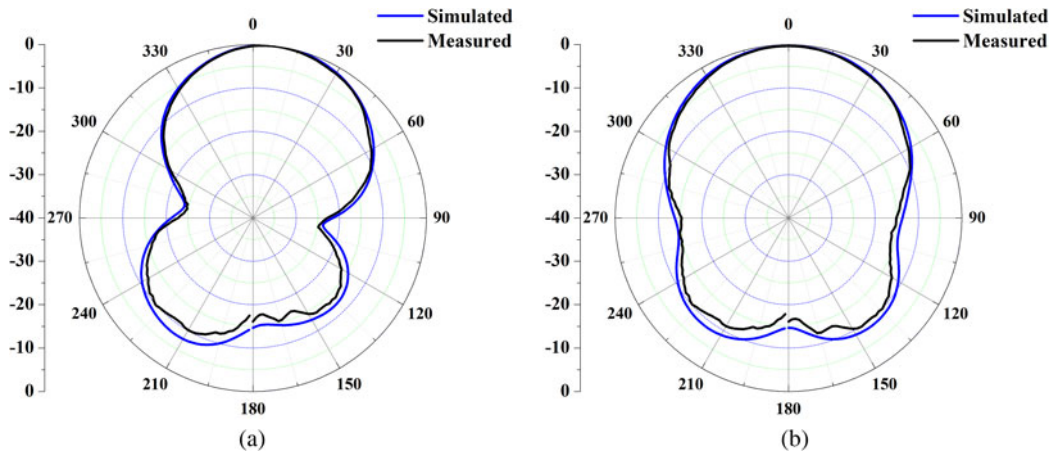

Figure 11. Radiation pattern of the integrated antenna in (a) *XZ* plane and (b) *YZ* plane.

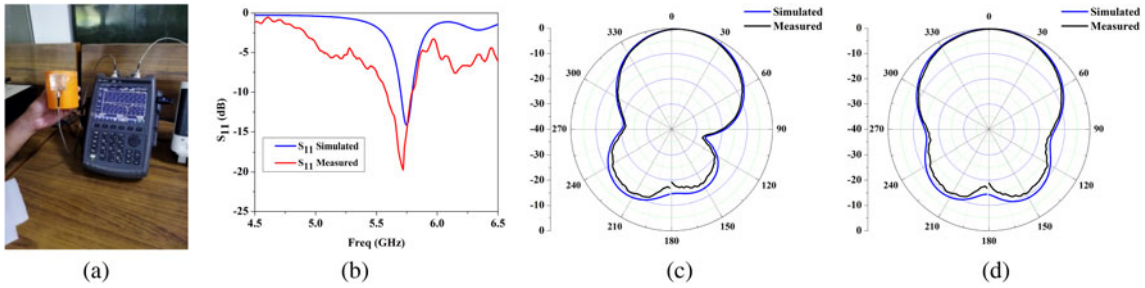

Figure 12. (a) Antenna testing under bending, (b) comparison between simulated and measured reflection coefficients for bending radius, rad = 40 mm, radiation pattern of the integrated antenna under bending in (c) *XZ* plane, and (d) *YZ* plane.

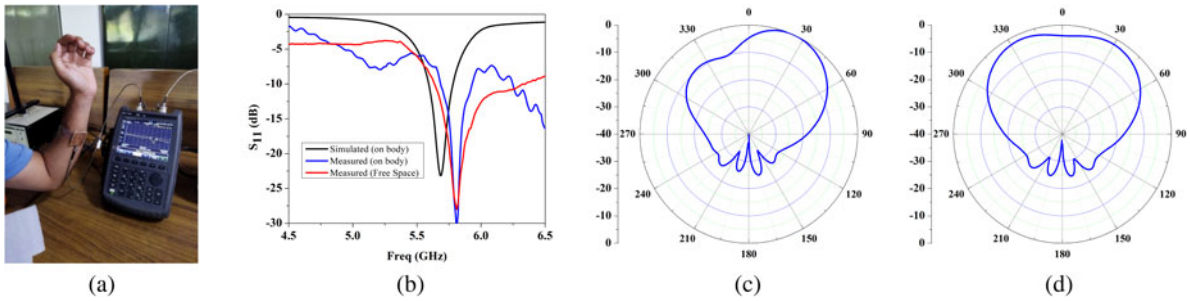

Figure 13. (a) On body measurement of reflection coefficient, (b) comparison between simulated and measured reflection coefficient, simulated radiation pattern in on body environment (c) *XZ* plane, and (d) *YZ* plane.

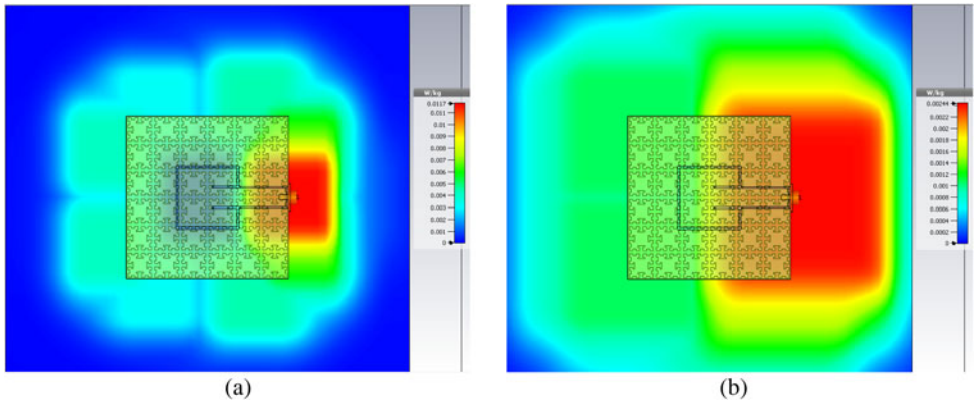

Figure 14. SAR calculations (a) averaged over 1 g, and (b) averaged over 10 g of human tissue.

https://doi.org/10.1017/S1759078723000211 Published online by Cambridge University Press

with the simulated ones as well as with free space measured results. It can be concluded from these results that the effect of frequency detuning due to the presence of the human body is well sustained by the antenna, and a sufficiently large impedance bandwidth of about 190 MHz still falls in the same ISM band with resonant frequency at 5.7 GHz. Moreover, measured results in both free space and the human body environment display a high degree of agreement, with resonant frequency being 5.82 GHz in both cases. Comparing these results of reflection coefficient with those presented in Fig. 4(b), which shows that the employment of AMC array as a backing element to the antenna, results in the reduction of the separation between human body and the antenna system from 12 to 0 mm.

Evaluation of gain and FBR on the human body

The simulated radiation pattern of the integrated antenna, when placed over the human body, is recorded and represented in *XZ* and *YZ* planes in Figs 13(c) and 13(d), respectively. The total realized gain and directivity of the antenna when placed over the human body model are found out to be 7.5 and 8.9 dBi, respectively, with an FBR of 32 dB. The radiation efficiency thus calculated from the values of directivity and gain using equation (1) comes out to be 84.28%.

$$G = \eta \times D \tag{1}$$

In equation (1), gain and directivity of the antenna are represented by G and D respectively, while η is used to represent the radiation efficiency of the antenna. The obtained values of gain, directivity, radiation efficiency, and FBR suggest the applicability of the proposed antenna for wearable applications.

SAR measurements

SAR signifies the rate of electromagnetic absorption into the human body and is expressed in the units of watts per kilogram. Looking from the point of view of human health, SAR is a very crucial parameter, and its value needs to be maintained within limits specified by Federal Communications Commission (FCC) and International Electro-technical Commission (IEC) for any antenna to qualify for WBAN applications. The permissible value of SAR according to FCC is 1.6 W/kg averaged over 1 g of human tissue, while according to the limits set by IEC, it is 2 W/kg averaged over 10 g of human tissue.

Equation (2) represents the mathematical expression of SAR in terms of electric field (E), conductivity (σ), and mass density (ρ) of the human tissue [19].

$$\text{SAR} = \frac{\sigma |E|^2}{\rho} \tag{2}$$

SAR values at 5.8 GHz as calculated in CST Microwave studio using IEEE/IEC 62704-1 averaging method [32] are 0.0117 W/kg, averaged over 1 g of human tissue, and 0.00244 W/kg, averaged over 10 g of human tissue. The pictorial representation of SAR results is depicted in Fig. 14.

Comparison with recent works

Performance comparison of the proposed antenna solution for WBAN applications with some of the recent state-of-the-art works reported in the literature is presented in Table 6. Taking into account the compactness of the proposed antenna system,

Table 6. Comparison with state-of-the-art literature

Ref.	*f* (GHz)	Physical size	Electrical size	Gain (dBi)	FBR (dB)	SAR (1 g/10 g)
This work	**5.8**	**36 × 36 × 3.8**	**$0.69\lambda_0 \times 0.69\lambda_0 \times 0.07\lambda_0$**	**7.5**	**32**	**0.0117/0.00244**
[20]	2.45, 3.3	88.75 × 82.5 × 9.3	$0.72\lambda_0 \times 0.67\lambda_0 \times 0.076\lambda_0$	6.4, 3	NA	0.29/NA
[21]	5.8	34.4 × 34.4 × 7	$0.66\lambda_0 \times 0.66\lambda_0 \times 0.13\lambda_0$	7.5	31.4	0.0264/0.014
[22]	2.45, 5.8	72 × 72 × 9	$0.59\lambda_0 \times 0.59\lambda_0 \times 0.073\lambda_0$	5.2, 7.7	NA	2.48/0.7
[19]	3.5, 5.8	86 × 86 × 5.6	$\lambda_0 \times \lambda_0 \times 0.065\lambda_0$	9.4, 6.6	14.4	0.0683/0.0226
[23]	2.4	50.7 × 25.7 × 11.2	$0.4\lambda_0 \times 0.2\lambda_0 \times 0.09\lambda_0$	4	NA	NA/1.8
[24]	2.45,3.5, 4.6, 5.8	90 × 90 × 26.2	$0.73\lambda_0 \times 0.73\lambda_0 \times 0.21\lambda_0$	4.93, 5.92, 5.54, 4.95	NA	NA
[25]	2.45	75.7 × 75.7 × 9.1	$0.62\lambda_0 \times 0.62\lambda_0 \times 0.074\lambda_0$	6.6	8.4	0.022/0.072
[26]	3.5, 5.8	45.3 × 45.3 × 7.8	$0.53\lambda_0 \times 0.53\lambda_0 \times 0.09\lambda_0$	6.7, 7.8	NA	$3.3 \times 10^{-6}/9.4 \times 10^{-7}$
[27]	2.45, 5.8	44.4 × 44.4 × 14.2	$0.36\lambda_0 \times 0.36\lambda_0 \times 0.116\lambda_0$	4.88, 4.73	NA	NA/0.9
[28]	3.5, 5.8	62 × 62 × 8.5	$0.72\lambda_0 \times 0.72\lambda_0 \times 0.099\lambda_0$	5.9, 6	18	0.043/NA

https://doi.org/10.1017/S1759078723000211 Published online by Cambridge University Press

higher gain, improved FBR, and low SAR values obtained from it, it may be recommended as a good candidate for employment in wearable communication industry.

Conclusion and future scope

A compact and economical integrated antenna, combining a CPW-fed monopole resonating at 5.8 GHz in the ISM band and a 6 × 6 array of a miniaturized AMC unit cell as a reflector surface, is presented in this article. AMC-backed monopole when placed over the human body equivalent model provided a total realized gain of 7.5 dBi with an FBR of 32 dB. The bandwidth of the proposed antenna system, when operated in the on body scenario, is measured to be 340 MHz, ranging from 5.68 to 6.02 GHz with resonance at 5.82 GHz. SAR, averaged over 1 and 10 g of human tissue, comes out to be 0.0117 and 0.00244 W/kg, respectively. The free space as well as on-body performance of the proposed design advocates strongly for its employment in wearable biomedical devices, as it conforms very well to all the performance parameters required for WBAN applications such as high gain, large FBR, low SAR, and a compact structure.

The concept of placement of the antenna element and AMC array on two different surfaces of the same substrate in order to reduce the usage of the expensive substrate and ultimately to propose an economical antenna solution for the wearable domain may be further utilized to propose multi-band antennas and MIMO antennas in future.

Acknowledgements. The authors are thankful to the supreme consciousness that pervades through each and every bit of the cosmos.

Author contributions. The concept and design of this study is envisaged by Mohit Yadav, Muquaddar Ali guided the simulation work, and R. P. Yadav supervised the experimental findings.

Financial support. This research received no specific grant from any funding agency, commercial or not-for-profit sectors.

Competing interests. None.

References

1. **Hall Y Peter S and Hao AA** (2012) *Propagation for Body-Centric Wireless Communications*. Norwood, MA, USA: Artech House.
2. **Abbasi A, Qammer H, Ur-Rehman M, Qaraqe K and Alomainy A** (2016) *Advances in Body-Centric Wireless Communication: Applications and State-of-the-Art*. London, UK: IET.
3. **Negra R, Jemili I and Belghith A** (2016) Wireless body area networks: applications and technologies. *Procedia Computer Science* **83**, 1274–1281.
4. **Hadjidj A, Souil M, Bouabdallah A, Challal Y and Owen H** (2013) Wireless sensor networks for rehabilitation applications: challenges and opportunities. *Journal of Network and Computer Applications* **36**, 1–15.
5. **Lin C, Chang C, Cheng YT, Member S and Jou CF** (2011) Development of a flexible SU-8/PDMS-based antenna. *IEEE Antennas and Wireless Propagation Letters* **10**, 1108–1111.
6. **Liao X, Dulle M, de Souza e Silva JM, Wehrspohn RB, Agarwal S, Förster S, Hou H, Smith P and Greiner A** (2019) High strength in combination with high toughness in robust and sustainable polymeric materials. *Science (80-.)* **366**, 1376–1379.
7. **Abbasi MAB, Nikolaou SS, Antoniades MA, Nikolić Stevanović M and Vryonides P** (2017) Compact EBG-backed planar monopole for BAN wearable applications. *IEEE Transactions on Antennas and Propagation* **65**, 453–463.
8. **El Hajj W, Person C and Wiart J** (2014) A novel investigation of a broadband integrated inverted-F antenna design; application for wearable antenna. *IEEE Transactions on Antennas and Propagation* **62**, 3843–3846.
9. **Yan S, Volskiy V and Vandenbosch GAE** (2017) Compact dual-band textile PIFA for 433-MHz/2.4-GHz ISM bands. *IEEE Antennas and Wireless Propagation Letters* **16**, 2436–2439.
10. **Alomainy A, Hao Y, Owadally A, Parini CG, Nechayev Y, Constantinou CC and Hall PS** (2007) Statistical analysis and performance evaluation for on-body radio propagation with microstrip patch antennas. *IEEE Transactions on Antennas and Propagation* **55**, 245–248.
11. **Sievenpiper D, Zhang L, Broas RFJ, Yablonovitch E and Alexopolous NG** (2000) High-impedance electromagnetic surfaces with a forbidden frequency band. *IEEE Transactions on Microwave Theory and Techniques* **48**, 620.
12. **Nakano H, Hitosugi K, Tatsuzawa N, Togashi D, Mimaki H and Yamauchi J** (2005) Effects on the radiation characteristics of using a corrugated reflector with a helical antenna and an electromagnetic band-gap reflector with a spiral antenna. *IEEE Transactions on Antennas and Propagation* **53**, 191–199.
13. **Nakano H, Kikkawa K, Kondo N, Iitsuka Y and Yamauchi J** (2009) Low-profile equiangular spiral antenna backed by an EBG reflector. *IEEE Transactions on Antennas and Propagation* **57**, 1309–1318.
14. **Foroozesh A and Shafai L** (2008) Application of combined electric- and magnetic-conductor ground planes for antenna performance enhancement. *Canadian Journal of Electrical and Computer Engineering* **33**, 87–98.
15. **Akhoondzadeh-Asl L, Kern DJ, Hall PS and Werner DH** (2007) Wideband dipoles on electromagnetic bandgap ground planes. *IEEE Transactions on Antennas and Propagation* **55**, 2426–2434.
16. **Yadav M, Ali M and Yadav RP** (2021) "Gain enhanced dual band antenna backed by dual band AMC surface for Wireless Body Area Network applications," *2021 IEEE Indian Conf. Antennas Propagation, InCAP 2021*, pp. 494–497. doi: 10.1109/InCAP52216.2021.9726271
17. **Palmeri R, Bevacqua MT, Morabito AF and Isernia T** (2018) Design of artificial-material-based antennas using inverse scattering techniques. *IEEE Transactions on Antennas and Propagation* **66**, 7076–7090.
18. **Dewan R, Rahim MK, Hamid MR, Yusoff MF, Samsuri NA, Murad NA and Kamardin K** (2017) Artificial magnetic conductor for various antenna applications: an overview. *International Journal of RF and Microwave Computer-Aided Engineering* **27**, 1–18.
19. **El Atrash M, Abdalla MA and Elhennawy HM** (2019) A wearable dual-band low profile high gain low SAR antenna AMC-backed for WBAN applications. *IEEE Transactions on Antennas and Propagation* **67**, 6378–6388.
20. **Saeed SM, Balanis CA, Birtcher CR, Durgun AC and Shaman HN** (2017) Wearable flexible reconfigurable antenna integrated with artificial magnetic conductor. *IEEE Antennas and Wireless Propagation Letters* **16**, 2396–2399.
21. **Chaouche YB, Nedil M, Ben Mabrouk I and Ramahi OM** (2017) A wearable circularly polarized antenna backed by AMC reflector for WBAN communications. *IEEE Access* **10**, 12838–12852.
22. **Wang M, Yang Z, Wu J, Bao J, Liu J, Cai L, Dang T, Zheng H and Li E** (2018) Investigation of SAR reduction using flexible antenna with metamaterial structure in wireless body area network. *IEEE Transactions on Antennas and Propagation* **66**, 3076–3086.
23. **El Atrash M, Abdalla MA and Elhennawy HM** (2021) A compact flexible textile artificial magnetic conductor-based wearable monopole antenna for low specific absorption rate wrist applications. *International Journal of Microwave and Wireless Technologies* **13**, 119–125.
24. **Gong Y, Yang S, Li B, Chen Y, Tong F and Yu C** (2020) Multi-band and high gain antenna using AMC ground characterized with four zero-phases of reflection coefficient. *IEEE Access* **8**, 171457–171468.
25. **El Atrash M, Abdalgalil OF, Mahmoud IS, Abdalla MA and Zahran SR** (2020) Wearable high gain low SAR antenna loaded with backed all-textile EBG for WBAN applications. *IET Microwaves, Antennas & Propagation* **14**, 791–799.
26. **El Atrash M, Abdalla MA and Elhennawy HM** (2021) A fully-textile wideband AMC-backed antenna for wristband WiMAX and medical applications. *International Journal of Microwave and Wireless Technologies* **13**, 624–633.
27. **Ahmad S, Paracha KN, Sheikh YA, Ghaffar A, Butt AD, Alibakhshikenari M, Soh PJ, Khan S and Falcone F** (2021) A metasurface-based single-layered compact AMC-backed dual-band antenna for off-body IoT devices. *IEEE Access* **9**, 159598–159615.

https://doi.org/10.1017/S1759078723000211 Published online by Cambridge University Press

28. **Yang H, Liu X, Fan Y and Xiong L** (2022) Dual-band textile antenna with dual circular polarizations using polarization rotation AMC for off-body communications. *IEEE Transactions on Antennas and Propagation* PP, 1.
29. **Dielectric Properties of Body Tissues**. Available at http://niremf.ifac.cnr.it/tissprop/ (accessed 15 June 2018).
30. **Body Tissue Dielectric Parameters**. Available at https://www.fcc.gov/general/body-tissue-dielectricparameters (accessed 15 June 2018).
31. **Density and Mass of Each Organ Tissue**. Available at http://bionumbers.hms.harvard.edu/bionumber.aspx?id=110245 (accessed 15 June 2018).
32. **IEEE/IEC 62704-1-2017 – IEC/IEEE international standard for determining the peak spatial average specific absorption rate (SAR) in the human body from wireless communications devices, 30 MHz–6 GHz. Part 1: general requirements for using the Finite**. Available at https://standards.ieee.org/standard/62704-1-2017.html (accessed 15 June 2018).

Mohit Yadav received B.Tech. degree in electronics and communication engineering from Dr. A. P. J. Abdul Kalam Technical University, Lucknow, India, in 2010, and M.Tech. degree from Madan Mohan Malaviya University of Technology, Gorakhpur, India, in 2014. With 5 years of academic experience as a teacher, he is currently pursuing Ph.D. at Malaviya National Institute of Technology, Jaipur, India. His research interests include microwave devices, microstrip antennas, and slot antennas.

Muquaddar Ali received B.Tech. degree in electronics and communication engineering from MLVTEC, Bhilwara, Rajasthan Technical University, Kota, India, in 2011, and M.Tech. degree from the Indian Institute of Technology Roorkee, India, in 2013. He earned the title of Ph.D. in the year 2022, from Malaviya National Institute of Technology, Jaipur, India. Currently he is working as an assistant professor with JECRC University, Jaipur. His research interests include microwave devices, substrate integrated waveguides, slot antennas, microstrip antennas, and beamforming networks.

Rajendra P. Yadav is currently working as a professor with the Department of Electronics and Communication Engineering, Malaviya National Institute of Technology, Jaipur, India. Besides being an able academician and administrator (Ex Vice Chancellor of Rajasthan Technical University, Kota and Ex Chairman NWRC Chandigarh AICTE), Rajendra is actively engaged in research in communication engineering, MEMS, MIMO-OFDM, multi user detection, microstrip antenna and arrays, optical communication, and engineering education.

https://doi.org/10.1017/S1759078723000211 Published online by Cambridge University Press